IOPscience iopscience.iop.org

Home Search Collections Journals About Contact us My IOPscience

Reaction mechanisms and thin a-C:H film growth from low energy hydrocarbon radicals

This article has been downloaded from IOPscience. Please scroll down to see the full text article.

2007 J. Phys.: Conf. Ser. 86 012020

(http://iopscience.iop.org/1742-6596/86/1/012020)

View the table of contents for this issue, or go to the journal homepage for more

Download details:
IP Address: 146.175.13.243
The article was downloaded on 26/06/2012 at 09:51

Please note that terms and conditions apply.

5th EU–Japan Joint Symposium on Plasma Processing IOP Publishing
Journal of Physics: Conference Series **86** (2007) 012020 doi:10.1088/1742-6596/86/1/012020

Reaction mechanisms and thin a-C:H film growth from low energy hydrocarbon radicals

E Neyts[1,3], A Bogaerts[1] and M C M van de Sanden[2]

[1] University of Antwerp, Department of Chemistry, PLASMANT Research Group, Universiteitsplein 1, 2610 Antwerp, Belgium
[2] Eindhoven University of Technology, Department of Applied Physics, Den Dolech 2, 5600 MB Eindhoven, The Netherlands

erik.neyts@ua.ac.be

Abstract. Molecular dynamics simulations using the Brenner potential have been performed to investigate reaction mechanisms of various hydrocarbon radicals with low kinetic energies on amorphous hydrogenated carbon (a-C:H) surfaces and to simulate thin a-C:H film growth. Experimental data from an expanding thermal plasma setup were used as input for the simulations. The hydrocarbon reaction mechanisms were studied both during growth of the films and on a set of surface sites specific for a-C:H surfaces. Thin film growth was studied using experimentally detected growth species. It is found that the reaction mechanisms and sticking coefficients are dependent on the specific surface sites, and the structural properties of the growth radicals. Furthermore, it is found that thin a-C:H films can be densified using an additional H-flux towards the substrate.

1. Introduction

Carbon forms a great variety of materials, ranging from crystalline to amorphous structures. This plethora of materials exists due to the different hybridisations carbon can exist in. Important carbon materials include crystalline diamond, in which the carbon atoms are sp^3 hybridised, and graphite, where the carbon atoms are sp^2 hybridised. Technological important materials also include carbon nanotubes, fullerenes, polymers, and a broad class of amorphous materials. The amorphous materials can be divided into those that consist of carbon only, and those that consist of carbon and one or several other materials, such as hydrogen, nitrogen, or metals. Even limiting ourselves here to those materials containing only carbon and hydrogen, many different classes of materials exist, each with their own specific properties.

1.1. Structure and growth mechanisms

Following Casiraghi [1], hydrogenated amorphous carbons (a-C:H) can be classified into four groups:

1. a-C:H films with the highest H-content (40-50%). These films can have sp^3 fractions up to 60%. However, most of the sp^3 bonds are H-terminated. Hence, there is no strongly interconnected sp^3-sp^3 network, and these films are soft and porous. Their hardness is usually below 10 GPa [2]. They are referred to as polymeric a-C:H (PLCH).

[3] To whom any correspondence should be addressed.

© 2007 IOP Publishing Ltd

2. a-C:H films with intermediate H-content (20-40%). Although these films have generally a lower sp^3 content, the C-C sp^3 network is more extensive as compared to PLCH films. Hence, these films are denser and harder. Hardness values of up to 20 GPa can be obtained [2]. They are often referred to as diamond-like a-C:H (DLCH).
3. ta-C:H, or hydrogenated tetrahedral amorphous carbon. They contain up to 70% sp^3 bonds, and a H-fraction of about 25%. These films have the highest density and hardness of all a-C:H's, with a hardness of up to 50 GPa [3].
4. a-C:H with low H-content (< 20%). They have a high sp^2 content, and are referred to as graphitic a-C:H, or GLCH. Their hardness is usually only a few GPa [4].

In the following, the term a-C:H is used to simply denote a film composed of carbon and hydrogen, without any further specifications. Note that in the literature, the term DLC has often been used wrongly for this purpose.

Obviously, the categories as given above are not defined by sharp boundaries. Furthermore, the overall structure is not necessarily homogeneous. For example, ta-C:H can locally contain crystalline fractions, embedded in a more amorphous matrix. DLCH can contain clusters of sp^2 carbons, embedded in a sp^3 matrix.

The growth mechanism of a-C:H films depends on the deposition technique used. When hard films are desired, the key property is the sp^3 fraction. The sp^3 matrix of hard DLCH and ta-C:H forms a rigid, strongly cross-linked network, determining the mechanical properties of the film. The deposition process which promotes sp^3 bonding is a physical process: ion bombardment [5-9]. The deposition mechanism of these hard films is currently understood in terms of the so-called "subplantation model". Robertson proposed that the subplantation creates a metastable increase in density, leading to a local change in bonding to sp^3 [10, 11]. Various simulations demonstrated the basic idea of subplantation, see *e.g.* [12-15]. Carbon ions in the energy range of 10-1000 eV can penetrate up to a few nm into the growing film, loosing their energy mainly by elastic collisions with the target atoms (nuclear stopping). Hence, the carbon ions penetrate the surface, and enter a subsurface interstitial site. This increases the local density. The local binding will then reform around that atom according to this new density. The whole process consists of three stages: (a) a collisional stage (~ 0.1 ps); (b) a thermalisation stage (~ 1 ps); (c) a relaxation stage (~ ns range). The thermalisation and relaxation stages are presumed to allow the excess density to relax again, causing a loss of sp^3 bonding at higher ion energies. At low ion energies, the increased sp^3 content is explained by the increased penetration probability. At high ion energies, the decreased sp^3 content is controlled by the relaxation. Although this model can explain the energy dependence of the sp^3 fraction, the relaxation stage of this process is not yet fully understood. Furthermore, the model cannot explain the transition temperature to sp^2 bonding at around 400-500 K, nor its dependence on the ion energy.

In the softer a-C(:H) films, the deposition mechanisms are different. In figure 1, a schematic drawing is shown indicating various processes occurring at an a-C:H surface. In contrast to ta-C deposition, the ion flux fraction is now much lower than 100%, and may be as low as only a few percents [2, 17]. The role of the ions remains the same as for the deposition of hard layers, i.e., increasing the sp^3 fraction by the subplantation mechanism. However, in systems involving not only ions, but also neutrals such as in plasma enhanced chemical vapor deposition (PECVD), the neutral species will also contribute to the growth. This is a chemical process, in contrast to subplantation, which is a physical process. Indeed, the contribution of each neutral species to the growth rate depends on its sticking coefficient, which is in turn determined by its chemical surface reactivity [16].

The a-C:H surface is essentially fully covered by C-H bonds, so it is chemically passive. Diradicals, such as CH_2, can insert directly into C-C and C-H surface bonds. Hence, these species have sticking coefficients approaching 1. Closed shell neutrals, on the other hand, such as CH_4, have very low sticking coefficients and their effect is negligible. Monoradicals, such as CH_3, have a moderate effect. They can react with the film surface if dangling bonds are present, since they cannot insert directly into surface bonds. These dangling bonds can be created by removal of H-atoms at the surface. Hydrogen atoms can be removed either by an ion displacing the H-atom, or by an H-atom

abstracting H from the C-H surface bond, or by an incoming radical such as CH_3. The latter mechanism is shown to be responsible for the synergistic effect of H on the sticking coefficient of CH_3 [18, 19].

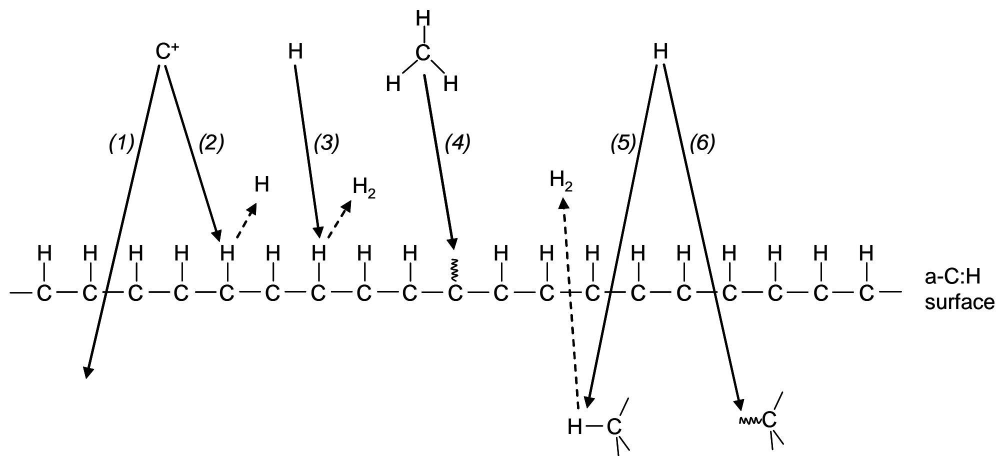

Figure 1 – Schematic representation of the deposition process in a-C:H film growth: ion subplantation (1); surface dangling bond creation by ion impact (2); surface dangling bond creation by H-abstraction (3); addition of radical on surface dangling bond (4); H-abstraction from subsurface C-H bonds (5); H repassivating subsurface dangling bonds (6).

Neutral hydrocarbon radicals can only react at the surface, since they are too large to penetrate into the layer. Hydrogen atoms, on the other hand, can penetrate about 2 nm into the film [20], where they can create subsurface dangling bonds, abstracting H from subsurface C-H bonds. In this way, H_2 is formed, which can desorb from the film or become trapped interstitially. In sources where no substrate bias used, and ion bombardment of the substrate is negligible, growth proceeds entirely through chemical surface reactions.

1.2. Properties and applications

The properties of the film determines the different possible applications. The mechanical properties of a-C:H are of great importance because of their extensive use as protective coatings. Mechanical properties include *e.g.* hardness, density, adhesion, wear and friction. The hardness of a-C(:H) varies from very soft (a few GPa) to very hard (up to values of 88 GPa) [16], and is mainly determined by the sp^3 fraction and the H-content. Closely related to the hardness is the density, varying between 1.2 $g.cm^{-3}$ for soft a-C:H films to 3.3 $g.cm^{-3}$ for superhard ta-C [7]. Since the main application of (hard) films is their use as protective coatings, a good adhesion to the substrate is crucial, requiring low compressive stresses. However, the compressive stress in the film is closely related to the hardness. Since films with high compressive stresses will easily delaminate, the compressive stress limits the maximum thickness of the film. Several solutions can be thought of to circumvent this problem, *e.g.* deposition of one or several adhesion layers prior to the a-C:H film deposition, or ion beam mixing between the film and the substrate in order to ensure a mixed interface [20, 21].

Amorphous carbon films are also notable for their low friction coefficients. For a-C:H, values as low as 0.01 [22] and 0.002 [23] have been reported. However, usually values between 0.02 and 0.15 are found for a-C:H. For comparison, the friction coefficient for steel on steel is about 0.8. It is believed that these low friction coefficients are due to the hydrophobic nature of the surface: contact with a different surface causes the formation of a transfer layer of a-C:H to be formed on the other surface. Thus, the contact is essentially between two hydrophobic a-C:H layers, which only interact with each other through van der Waals forces. The surface of ta-C on the other hand is believed to

transform into graphitic layers upon contact and wear. These mechanisms also account for the resistance of these films to wear.

a-C:H films also show excellent chemical resistance. At room temperature, a-C:H films are chemically inert to practically any solvent, acid or base. Because of this chemical resistance and their continuity, a-C:H films can be used as corrosion-resistant coatings [19].

These mechanical, tribological and chemical properties enable amorphous carbons to be used in a variety of applications. As mentioned above, one of the main applications is their use as protective coatings, *e.g.* on magnetic hard discs. a-C:H is used because it can be made very thin, and it exhibits an extreme smoothness, it is continuous and chemically inert. Presently, there are no competitors as a coating material for this application. They are also used as protective coatings on *e.g.* razor blades, sunglasses [24] and bar-code scanners. This is possible due to the optical transparancy of a-C:H in the IR region (apart from the absorbing C-H bands). Furthermore, a-C:H can also be used as biocompatible coatings on parts such as hip joints, hart valves and stents, due to the fact that the carbon material is biocompatible, has a low friction coefficient, and does not produce metallic wear debris [25, 26]. Finally, a-C:H's are also used in electronic applications, although to a much lesser extent. One example is their use as antifuses. An antifuse changes from high to low electrical resistance when there passes a large current. This process in a-C's is believed to involve a change to more sp^2 bonding as the large current passes. Amorphous carbons have been shown to make useful antifuses [27, 28].

1.3. Deposition techniques

As mentioned above, various types of films can be deposited depending on the type of deposition source used. The most popular techniques include ion beam deposition (IB), sputtering and PECVD. The first DLC films were produced in 1971 by Aisenberg and Chabot using ion beam deposition [29]. In fact, ion beam deposition is a term used to group several similar deposition techniques. The common feature of these techniques is to use a beam of carbon or hydrocarbon ions with medium energy (tens to hundreds of eV). Typically, the ions are produced by plasma sputtering of a graphitic cathode in an ion source [29, 30]. Alternatively, a hydrocarbon gas can be ionised in a plasma [31, 32]. The ion beam can then be extracted from the plasma source through a grid by a bias voltage. The ions are accelerated in a high vacuum deposition chamber to form the actual ion beam. Since the ion source runs at finite pressure, the beam also contains a fraction of neutral species. Typically, ion beam deposition systems produce films that are hard, dense and have a low surface roughness. Hence, films produced by these sources are well suited for use as protective coatings.

The most common industrial deposition technique for amorphous carbons is sputter deposition [33, 34]. The central idea is to sputter material from a graphite electrode, which can deposit on the substrate. The sputtering is accomplished by an Ar plasma, or, as in ion beam sputtering, by an Ar ion beam. A second Ar ion beam can be used to bombard the growing film. This is called ion beam assisted deposition [35]. Sputter sources generally have a rather low ion to neutral flux ratio towards the substrate, such that very hard films cannot be produced in these sources. On the other hand, these sources are very versatile and are easy to scale up. Also, the deposition conditions can be controlled by the plasma power and the pressure, and they are reasonably independent of the substrate geometry.

One of the most popular (laboratory) deposition techniques nowadays is radio frequency PECVD [36, 37]. While in IB the substrate is placed in a deposition chamber separated from the ion source, in PECVD the substrate is mounted on one of the electrodes in the same reactor where the species are created. The reactor consists of two electrodes of different area. The substrate is placed on the smaller electrode, to which the power is capacitively coupled. Since the smaller electrode acquires a larger bias voltage and becomes negative with respect to the larger electrode, the negative sheath voltage at the smaller electrode will accelerate the positive ions towards this electrode on which the substrate is mounted, promoting the sp^3 bonding. In order to maximize the ion to neutral ratio in the plasma, the plasma must be operated at the lowest possible pressure. Nevertheless, the ions are only about 10 percent of the film-forming flux even at pressures as low as 50 mTorr. Lower pressures cannot be used

as the plasma will not longer strike. A second disadvantage of this source is the energy spread in the ion energy distribution, prohibiting a controlled deposition. Yet another disadvantage of the rf PEVCD source is that it is not possible to have independent control over the ion energy and flux, as they both vary with the rf power. On the other hand, PECVD allows the deposition of uniform films over large areas, and PECVD systems can be easily scaled up. Films deposited by this source are generally medium hard, up to values of 30 GPa [38]. In order to overcome the disadvantages of rf PECVD, several similar techniques have been developed. Examples include microwave induced PECVD, allowing for a lower gas pressure and a higher ion to neutral ratio [39], and electon cyclotron resonance microwave plasma CVD (ECR-MPCVD). The latter technique also allows for a higher plasma density, and control over the ion energy separately from the ion flux [40-42].

Finally, another variant of the PECVD technique is the expanding thermal plasma (ETP). The ETP is a remote source, consisting of two parts: a cascaded arc in which the plasma is created, and a reactor chamber, in which the substrate is placed [43]. A schematic drawing of the set-up is shown in figure 2.

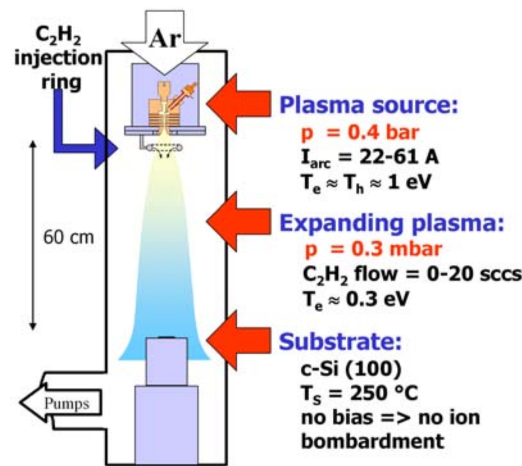

Figure 2 – Schematic drawing of the ETP set-up.

An Ar thermal plasma is created in the cascaded arc plasma source, operated at sub-atmospheric pressure. The argon plasma expands into the low pressure reaction vessel. At the top of the reaction vessel an injection ring is placed. The hydrocarbon gas is admixed into the emanating plasma by means of this injection ring. In the expanding plasma, many chemical reactions take place, and the growth species are created. These species subsequently reach the substrate where they can deposit.

In [44-50], the ETP source was used with acetylene as the hydrocarbon gas. Since no substrate bias was applied, ion bombardment of the substrate is precluded. Nevertheless, medium hard films could be obtained with a hardness of 14 GPa, Young's modulus of 120 GPa, a refractive index of 2.2 and a density of 1.7 g.cm^{-3}. Furthermore, the films showed good adhesion on glass and crystalline silicon, as well as chemical stability. The main advantage of this technique, however, is the ultra-high deposition rate of 70 nm.s^{-1}. It has also been shown that the film quality is improved under high deposition rate conditions [45, 46]. Several studies have been carried out to elucidate the plasma chemistry and the growth species generation [46-50]. It was determined that the crucial factors determining the film properties, as well as the growth rate, were the arc current and the acetylene loading. The type of growth species that are created in the expanding plasma, is determined by the ratio between the fluxes of the acetylene and the Ar^+ ions:

$$F = \frac{\Phi_{C_2H_2}}{\Phi_{Ar^+}}$$

When the C_2H_2 flow is smaller than the argon ion and electron fluence emanating from the plasma source, i.e., $F < 1$, the acetylene is fully decomposed by the plasma reactions, leading to the formation of C, CH, CH_2, C_2 and C_2H. C and C_2 radicals have the highest densities, and are presumed to be responsible for the growth of soft, polymer-like a-C:H films formed under these conditions [47]. When the acetylene flow is higher than the argon ion and electron fluence emanating from the plasma source, i.e., $F > 1$, the acetylene is only partially decomposed into C, CH, CH_2, C_2 and C_2H. Under these conditions, the C_2 and C_2H radicals can react with the remaining C_2H_2 leading to the formation of C_4, C_4H and C_4H_2. The C and CH radicals on the other hand react with C_2H_2 leading to the formation of mainly C_3 and C_3H. These species are unreactive in the gas phase. It was shown that the C_3 radical has the highest density in the region close to the substrate, and its density was correlated with the measured growth rate. Since its surface reactivity was previously already reported to be high [51], it was suggested that the C_3 radical is probably responsible for the fast growth of hard a-C:H films under $F > 1$ conditions. However, it was also found that the stoichiometry of the film could not be explained by the carbon containing growth species alone. Hence, it was concluded that additional hydrogen has to be incorporated into the film during the growth.

Although most of the plasma chemistry in the ETP was elucidated, and the important (presumed) growth species have been identified, the actual growth process remains unclear. More specifically, questions remain regarding the actual growth mechanism, the surface reactions, and the role of the additional hydrogen during film growth. In this paper, we have investigated the above mentioned growth mechanisms and film growth by means of molecular dynamics (MD) computer simulations. In the following section, the simulation model will be described. In section 3, we will summarize the results of the reaction mechanisms as determined for various hydrocarbon radicals. In section 4, the results will be presented for the simulated film growth under $F < 1$ conditions. Finally, a conclusion will be given.

2. Description of the simulation model

The model used for this study, is a classical molecular dynamics (MD) model. The model was originally developed by Tanaka *et al.* [52]. The interatomic potential used in these simulations is the well known Brenner potential for hydrocarbons [53]. In the MD methodology, the atoms in the system are followed through space and time by integrating Newton's law. The atoms move under the influence of forces derived from the interatomic potential. The integration scheme used is the velocity-Verlet algorithm [54]. The time step used is invariably set to 0.2 fs.

In a first set of simulations, the reaction mechanisms of selected hydrocarbons were investigated on various surface sites. The hydrocarbons included were C_2, linear C_3, linear C_3H and cyclic C_3H. The surface itself is either a non-passivated, non-reconstructed diamond {111} surface, or a H-passivated non-reconstructed diamond {111} surface. A site is defined as a specific location on this surface: it can be a dangling bond, or one or several atoms bound on top of the diamond surface, corresponding to sites as they are grown during a deposition process. The main difference between a diamond substrate containing specific a-C:H sites (as used in this work), and a 'true' a-C:H surface, is the bond angle and bond length distribution, possibly influencing the site-specific system reactivity. The current model system was chosen in order to obtain a well defined system. Initially, the substrate was relaxed at 100 K using the Berendsen heat bath algorithm [55]. The hydrocarbon radical is placed at a specified $\{x, y\}$ position above the site of interest beyond the cut-off of the potential. The atoms in the substrate are allowed to move freely, except for the site-atoms. These are kept fixed, until the potential energy between one of the site-atoms and the hydrocarbon radical becomes negative, in order to make sure that the radical impinges exactly on the required position on the site. During the impact, no heat bath is applied. The radicals were given a kinetic energy of 0.13 eV, corresponding to the experimentally determined gas temperature of about 1500 K [49].

In a second set of simulations, the growth process of a-C:H films was simulated using experimentally detected hydrocarbon radicals as the growth species. These species and their relative fluxes are given in Table 1. Since the flux of hydrogen towards the substrate could not be measured

experimentally, a relative H-flux ($\Phi_{H, rel}$) was used in the range between 0 and 45%. Again, the kinetic energy of the species was set to 0.13 eV. In these growth simulations, a clean diamond {111} surface is exposed to consecutive particle impacts. Each impact was followed for 2 ps, applying a heat bath set at 100 K during the last 0.4 ps. The output of every impact is the input for the next impact. After each impact, unbound atoms are removed from the configuration. Growth was continued until the films reached a thickness of about 10 nm, each containing about 4000 atoms. After the growth phase, the films were allowed to relax for another 10 ps.

Table 1. Growth species and their fluxes.

Species	Relative flux
C	$0.71(1-\Phi_{H, rel})$
CH	$0.05(1-\Phi_{H, rel})$
C_2	$0.20(1-\Phi_{H, rel})$
C_2H	$0.04(1-\Phi_{H, rel})$
H	$\Phi_{H, rel}$

Although we have previously applied this model succesfully to study the deposition of thin a-C:H films and the reaction mechanisms of hydrocarbon radicals (see e.g. [56-58]), the model also has several shortcommings. First, surface diffusion of atoms is currently not yet taken into account. As a result of this, the deposition rate in the simulation is orders of magnitude higher compared to the experiment, since the time between impacts – during which diffusion could occur – is ignored in the simulation. Second, the Brenner potential as used in this work does not take into account intermolecular forces. Third, the kinetic energy of the impinging particles is very low, requiring a long simulation time to allow for sufficient relaxation of the resulting structure. Finally, it should also be noted that the reaction mechanisms determined by classical MD are very sensitive to the exact potential energy surface used, possibly requiring a potential more accurate than the Brenner potential.

3. Reaction mechanisms of hydrocarbon radicals on typical a-C:H sites

Using the model described above, reaction mechanisms of C_2, linear C_3, linear C_3H and cyclic C_3H were determined on 11 predetermined a-C:H sites. In the following sections, examples are given on how certain parameters specific for the reacting species, such as chemical connectivity and structural stability, as well parameters specific for the a-C:H sites, such as steric hindrance, affect the reaction behaviour. A more detailed discussion of the results can be found in [59].

3.1. Steric hindrance

Let us consider as a first example the impact of a linear C_3 radical on two a-C:H sites, shown in figure 3. The first site is a non-passivated diamond {111} surface covered with dangling bonds (labelled (a) in figure 3). The second site is a H-passivated diamond {111} substrate, with one dangling bond (labelled (b) in figure 3).

The calculated reflection coefficient of C_3 on the first site is 0.01, while on the second site it is 0.23. The radical is reflected more often on the second site due to steric hindrance: the H-atoms on the surface prevent the bulky C_3 from reaching the dangling bond. This also results in different sticking configurations of the radical: while the C_3 radical is observed to stick in only one configuration on site (b), five different configurations are found on site (a).

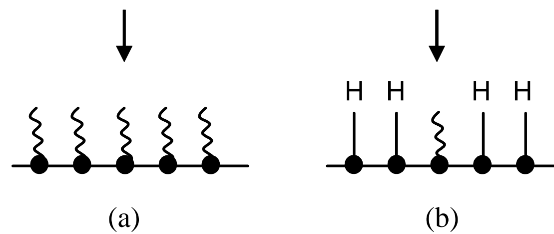

Figure 3 – 2D representation of two a-C:H sites. The wavy lines represent dangling bonds. The arrows indicate the impact position of the impinging radical.

Indeed, in 73% of the impacts on site (a), the C_3 radical binds to the surface with the formation of a single bond, and in the majority of these cases, this occurs with one of the two terminating C-atoms (61% vs. 12% with the middle C-atom). In 26% of the impacts, the radical binds to the surface with the formation of two bonds, either involving only the terminating C-atoms (22%), or both with the middle and one of the terminating C-atoms (4%). In 21% of the impacts, sticking occurs with the formation of a 'bridge' structure, as shown in figure 4. As mentioned above, in the remaining 1% of the impacts of C_3 on site (a), the radical is reflected.

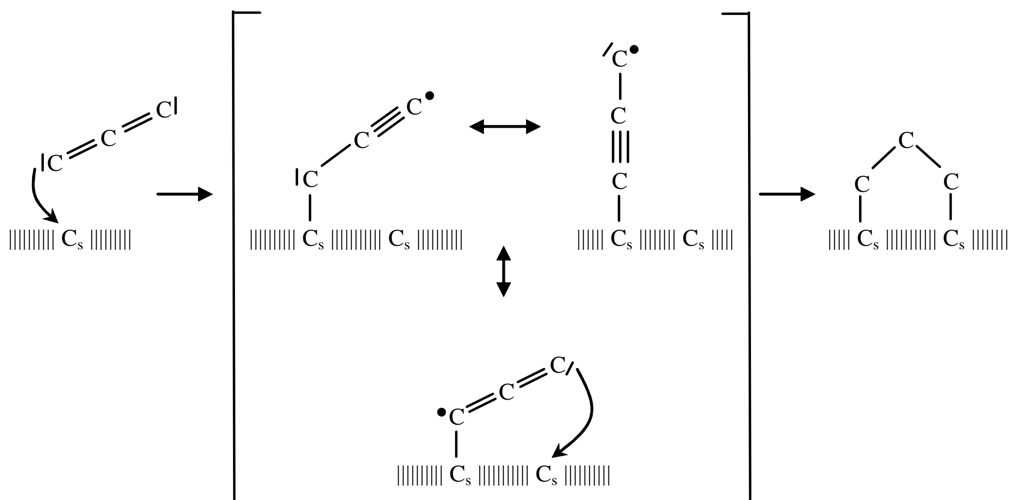

Figure 4 – Impact of C_3 leading to bridge formation on site (a) (see figure 3).

In nearly all investigated cases, we have observed that the site on which a specific radical sticks, affects both the total sticking coefficient of that species, as well as the number and structure of the various resulting configurations.

3.2. Species specific factors

Species specific factors are those that influence the sticking behaviour as determined by the properties of the impinging species, rather than due to the site on which the particle impinges. The examples below indicate how sticking affects the structure of the radical, and how the structural stability and the chemical connectivity in turn influence the sticking behaviour.

Consider a C_2 radical impinging a dangling bond on the surface. The Brenner potential predicts the C_2 radical in the gas phase to have a double C-C bond with a bond energy of 5.98 eV, leaving a lone pair of electrons on both C-atoms. Upon sticking, a single C-C bond is formed between the surface C-atom and one of the C-atoms of the radical. A plot of the binding energy evolution vs. time is shown in figure 5. In the figure, it can be seen how a single bond to the surface is formed with a bond energy of about 3.5 eV. The intramolecular C-C bond becomes stronger upon sticking by almost 2 eV, indicating the change of sp^2 hybridization in the gas phase (double C-C bond) to sp^1 hybridization upon sticking (triple C-C bond).

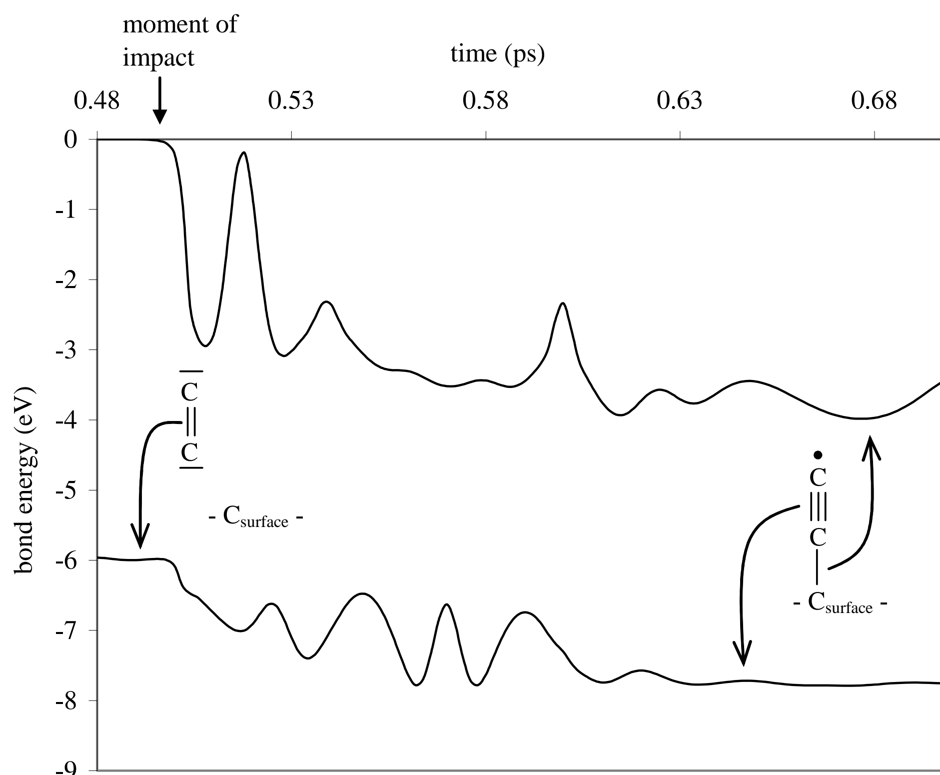

Figure 5 – Bond energy evolution of the $C_{surface} – C_{radical}$ bond and the intramolecular $C_{radical} – C_{radical}$ bond.

As a second example, consider the impact of a cyclic C_3H radical. Averaged over the total number of impacts on all investigated sites, the cyclic C_3H radical has a sticking coefficient of about 0.75, while the linear C_3H isomer has a sticking coefficient of about 0.40. There are two factors responsible for this difference.

First, it should be noted that the cyclic isomer is structurally unstable. This can be easily seen by comparing cyclopropane to *n*-propane: in cyclopropane, the C-C bonds are about 32% weaker than in the linear isomer, due to a severe ring strain of 117 kJ/mol. In cyclic C_3H, the effect is even more pronounced: the C-C bonds in cyclic C_3H are about 50% weaker than in linear C_3H. Hence, the release of this ring strain is a driving force for the radical to break up, enhancing drastically its reactivity. This breaking up of the molecule occurred in more than 70% of its sticking events.

The second reason is the fact that in the cyclic isomer, all three C-atoms bear electrons not participating in a bond, while in the linear isomer, the middle C-atom is fully bound by two double bonds. Hence, all three C-atoms in the cyclic isomer can potentially bind to the surface, while the

middle C-atom in the linear isomer experiences repulsive forces from the surface upon impact, and hence will not bind to the surface.

The breaking up of a cyclic C_3H can occur in several distinct ways. These mechanisms were observed on all investigated sites. The main effect of a break-up event, is the transformation of a cyclic structure into a linear one. The remaining bonds become stronger, depending on which bond is broken and which atom sticks to the surface. An example is shown in figure 6, schematically showing how one of the C-atoms of the radical becomes 3-coordinated upon sticking and break up. In the resulting configuration, the middle C-atom of the radical is now connected to the surface. As mentioned above, this does not occur when a linear radical sticks to the surface. Hence, when depositing a-C:H films using C_3H radicals as growth species, the connectivity of the film will be determined by which isomer (i.e., linear or cyclic) is present.

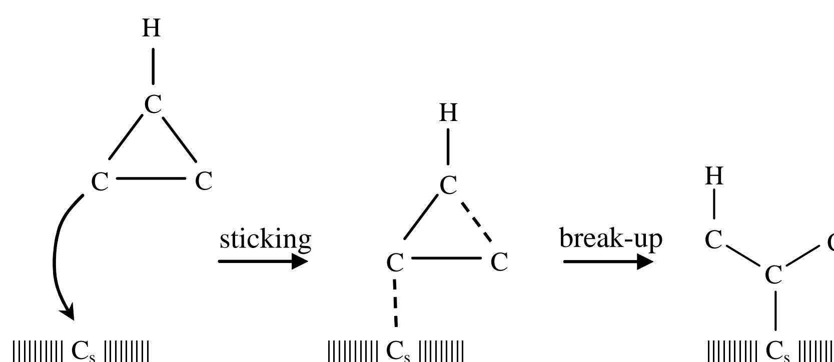

Figure 6 – Schematic representation of the sticking and breaking up of a cyclic C_3H radical, leaving the surface binding atom 3-coordinated.

As a final example, consider the impact of linear C_3 vs. linear C_3H. On average, the C_3 radical is about 10% more reactive compared to the C_3H radical. Both radicals have a fully bound central C-atom, which does not bind to the surface. The two other C-atoms, however, both have at least one unbound electron, and hence are available for direct sticking to a dangling bond. Structurally, the difference between both radicals is the presence of the H-atom on the C_3H radical. This limits the availability of the C-atom to which this H-atom is connected for sticking. In other words, the H-atom shields the C-atom to which this H-atom is connected for sticking to the surface.

4. Thin a-C:H film growth from low kinetic energy hydrocarbon radicals

Besides the investigation of the possible reaction mechanisms of hydrocarbon radicals on a-C:H sites, also the actual deposition process of a-C:H films was simulated using the growth species given in table 1. More information regarding these simulations can be found in [56].

In figure 7, the calculated H-content in the deposited films is shown as a function of the H-flux towards the substrate during growth. It can be seen in the figure that the uptake of hydrogen is nearly a linear function of the H-flux. This H-uptake in the films determines the fractions of CH_x fragments in the films, as shown in figure 8. Note that the formation of bulky CH_2 groups only occurs at a H-content in the film of about 25% or more. The H-uptake in the film and the concurrent formation of the CH_x fragments induces an increase in the mass density and atom density as described below.

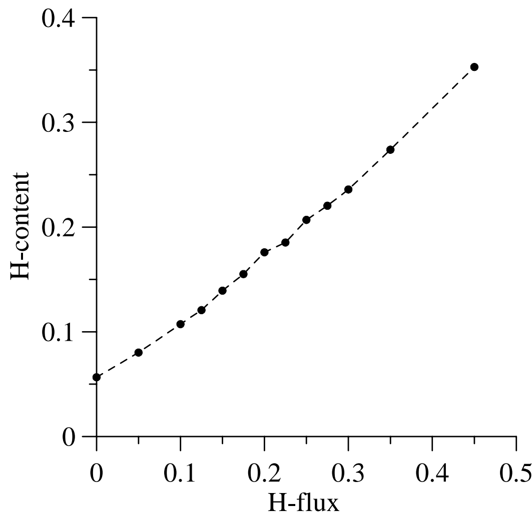

Figure 7 – Calculated H-content as a function of the H-flux towards the substrate.

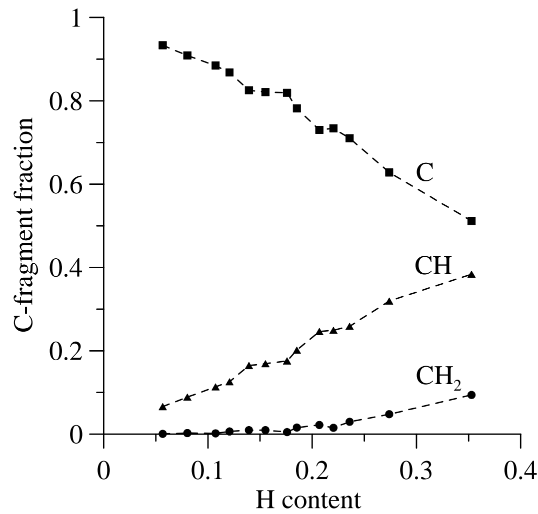

Figure 8 – Calculated fraction of CH_x fragments as a function of the H-content.

Previously, Ferrari *et al.* have already shown the decrease in mass density of a-C:H films with increasing H-content for films containing more than 40% sp^3 content (see [60] and references therein). In figure 9, it is shown that this effect also occurs under the conditions used in this study for high enough H-fluxes. The figure shows the calculated mass density and atom density of the different films as a function of the H-content in the bulk of the films. At low H-fluxes, little H is present in the film, and the mass density increases as a function of the H-content, until a maximum is found at a H-content of about 10%. The atom density, on the other hand, continues to increase as a function of the H-content. Indeed, a high H-flux allows the incorporation of a large H-fraction into the carbon matrix, increasing the atom density. This, however, does not increase the mass density due to the low H mass.

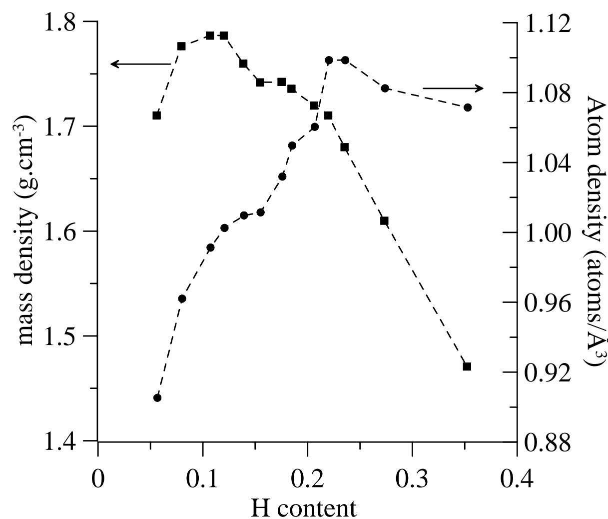

Figure 9 – Calculated mass densities and atom densities as a function of the H-content in the films.

As can be seen in figure 9, a maximum in the atom density is found at a H-content of about 22%, corresponding to a H-flux towards the substrate of about 30% (see figure 7). The occurrence of the bulky CH_2 groups at high H-fluxes (see figure 8) accounts for the decrease in both the mass density and atom density at a H-content > 25%. Also, as more H is incorporated in the film, relatively less C atoms must accommodate relatively more H-atoms, increasing the average carbon coordination number, in the range of 2.8-3.1 for a H-flux varying between 0% and 45%.

The observed increase in mass density with increasing H-content at low H-fluxes is explained by the changing hybridisation state of the carbon matrix. Indeed, the uptake of H into the films also considerably changes the microstructure of the films. In figure 10, the evolution of the sp^1, sp^2 and sp^3 C-sites in the bulk of the film is shown as a function of the H-content. A C-atom is considered to be sp^1 hybridized if it is one- or two-coordinated. Similarly, sp^2 and sp^3 carbon atoms are identified as three-coordinated and four-coordinated carbon atoms, respectively. It can be seen in the figure that increasing the H-content in the film decreases the sp^1 content, and increases the sp^2 content. This transition of sp^1 to sp^2 bonding as a function of the H-content coincides with the increase in mass density at low H-fluxes. In this region, the film structure is composed of a network of sp^2-like C-C bonds, stabilized by chemical resonance. As the sp^1 sites occupy a larger volume per atom than the sp^2 sites (sp^1 sites are linear, one-dimensional structures while sp^2 sites are two-dimensional), the sp^1 to sp^2 transition effectively lowers the volume per atom, and hence increases the mass density.

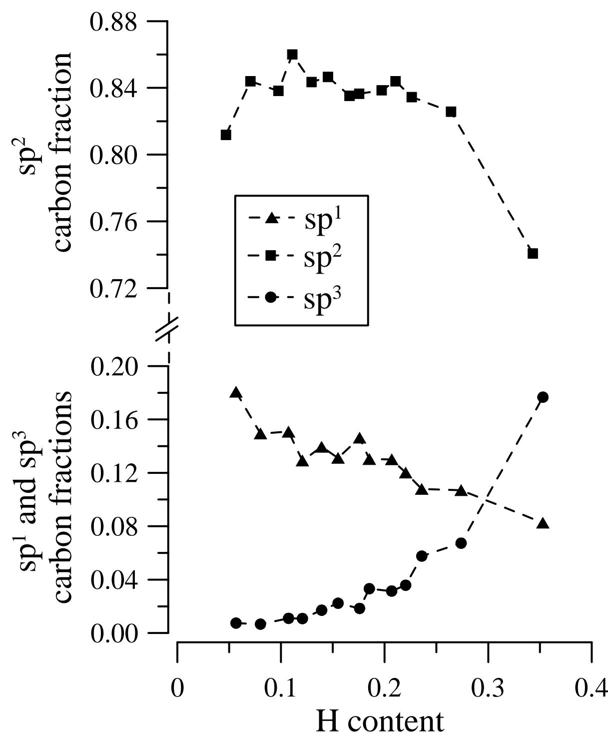

Figure 10 – Calculated sp^1, sp^2 and sp^3 fractions in the films as a function of the H-content.

Higher H-fluxes further lower the sp^1 content and strongly increase the sp^3 content, whereas the sp^2 content remains more or less constant. In this region, a considerable fraction of the film volume is taken by the H-atoms, contributing only to the atom density, and hardly to the mass density. Hence, the films now become more porous and less dense.

At even higher H-fluxes ($\Phi_{H,rel} > 0.30$), the sp^2 carbon atoms are converted into sp^3 carbons, coinciding with the maximum in the atom density. As mentioned above and as can be seen in figure 8, the fraction of bulky CH_2 groups now becomes important. These groups repel each other, such that from this point on, both the atom density and the mass density decrease. Hence, as the H-flux towards the substrate increases, there is a H-induced sp^1 to sp^2 to sp^3 shift.

As mentioned before, the H-flux towards the substrate could not be determined experimentally. From these simulations, however, an estimate can be made. The films deposited experimentally under conditions corresponding to the current simulation, show a H-content of about 33%, and a mass density of about 1.5 $g.cm^{-3}$. As can be seen from figure 9, our simulated result corresponds to the experimental result.

5. Conclusions

Thin amorphous hydrogenated carbon (a-C:H) films are important technological materials that are used in various applications. Because of their importance, various methodologies have been and are still used to investigate their properties and deposition mechanisms. In this paper, we have shown how classical molecular dynamics simulations can aid in deepening our understanding.

As a first application of these simulations, the reaction mechanisms of various hydrocarbon radicals on typical a-C:H sites were investigated. The species were chosen on the basis of an experimental expanding thermal plasma set-up. Examples are given of how both site-specific factors as well as species-specific factors contribute to the reaction behaviour of the radicals, including steric hindrance at the surface, chemical connectivity of the radical and the structural stability of the radical.

Second, thin a-C:H film growth was also simulated, corresponding to expanding thermal plasma conditions. It is shown how low hydrogen fluxes towards the substrate can induce a microstructural change in the film, leading to an increase in the mass density and atom density of the film. Higher H-fluxes result in a decrease of the mass and atom density of the film. Finally, also the H-flux towards the substrate that could not be measured experimentally, can be obtained from the simulation results.

Acknowledgments

One of the authors (E. Neyts) is indebted to the Institute for the Promotion of Innovation by Science and Technology in Flanders (IWT-Flanders) for financial support. The authors would also like to thank J. Benedikt for the many fruitful discussions on the chemistry in the expanding thermal plasma and the deposition mechanisms.

References

[1] Casiraghi C, Piazza F, Ferrari A C, Grambole D and Robertson J 2005 *Diamond Relat. Mater.* **14** 1098
[2] Koidl P, Wagner C, Dishler B, Wagner J and Ramsteiner M 1990 *Mater. Sci. Forum* **52** 41
[3] Weiler M, Sattel S, Jung K, Ehrhardt H, Veerasamy V S and Roberson J 1994 *Appl. Phys. Lett.* **64** 2797
[4] Robertson J 1986 *Adv. in Phys.* **35** 317
[5] McKenzie D R 1996 *Rep. Prog. Phys.* **59** 1611
[6] Lifshitz Y 1996 *Diamond Relat. Mater.* **5** 388
[7] Lifshitz Y 1999 *Diamond Relat. Mater.* **8** 1659
[8] Fallon P J, Veerasamy V S, Davis C A, Robertson J, Amaratunga G A J, Milne W I and Koskinen J 1993 *Phys. Rev.* B **48** 4777
[9] Robertson J 1994 *Pure Appl. Chem.* **66** 1789
[10] Robertson J 1993 *Philos. Trans. R. Soc. London* A **342** 277
[11] Robertson J 1994 *Diamond Relat. Mater.* **3** 361
[12] Kaukonen H P and Nieminen R M 1992 *Phys. Rev. Lett.* **68** 620
[13] Kaukonen H P and Nieminen R M 2000 *Phys. Rev.* B **61** 2806

[14] Marks N A 1997 *Phys. Rev* B **56** 2441
[15] Uhlmann S, Frauenheim T and Lifshitz Y 1998 *Phys. Rev. Lett.* **81** 641
[16] Robertson J 2002 *Mater. Sci. Eng.* R **37** 129
[17] Catherine Y 1991 *Diamond and Diamond-like Carbon Thin Films (NATO ASI Series: Series B: Physics* vol 266*)* ed Clausing R E *et al* (New York: Plenum Press) p 193
[18] Hopf C, Schwarz-Sellinger T and von Keudell A 2000 *J. Appl. Phys.* **87** 2719
[19] von Keudell A, Schwarz-Sellinger T and Jacob W 2001 *J. Appl. Phys.* **89** 2979
[20] Ugolini D, Eitle J and Oelhafen P 1990 *Vacuum* **41** 1374
[21] Antilla A, Lappalainen R, Tiainen V M and Hakovirta M 1997 *Acta Mater.* **9** 1161
[22] Erdemir A, Eryilmaz O L, Nilufer I B and Fenske G R 2000 *Diamond Relat. Mater.* **9** 632
[23] Fontaine J, Belin M, Mogne T L and Grill A 2004 *Tribol. Int.* **37** 869
[24] Kimock F M and Knapp B J 1993 *Surf. Coatings Technol.* **56** 273
[25] Yang P, Kwok S C H, Fu R K Y, Leng Y X, Wang J, Wan G J, Huang N, Leng Y and Chu P K 2004 *Surf. Coatings Technol.* **177-178** 747
[26] Jones M I, McColl I R, Grand D M, Parker K G and Parker T L 1999 *Diamond Relat. Mater.* **8** 457
[27] Liu S, Lamp D, Gangopadhyay S, Sreenivas G, Ang S S and Naseem H A 1998 *IEEE Ed. Lett.* **19** 317
[28] McKenzie D R, Li W T and Gerstner E G 2001 *Diamond Relat. Mater.* **10** 230
[29] Aisenberg S and Chabot R 1971 *J. Appl. Phys.* **42** 2953
[30] Druz B, Zaritskiy I, Yevtukhov Y, Konchits A, Valakh M, Shanina B, Kolesnik S, Yanchuk I and Gromovoy Y 2004 *Diamond Relat. Mater.* **13** 1592
[31] Kaufmann H R 1978 *J. Vac. Sci. Technol.* **15** 272
[32] Druz B, Ostan R, Distefano S, Hayes A, Kanarov V and Polyakov V 1998 *Diamond Relat. Mater.* **7** 965
[33] Jansen F, Mackonkin M, Kaplan S and Hark S 1985 *J. Vac. Sci. Technol.* A **3** 605
[34] Logothetidis S 1996 *Appl. Phys. Lett.* **69** 158
[35] Lacerda R G, Hammer P, Freire F L, Alvarez F and Marques F C 2000 *Diamond Relat. Mater.* **9** 796
[36] Valentini L, Kenny J M, Mariotto G and Tosi P 2001 *J. Mater. Sci.* **36** 5295
[37] Conway N M J, Ferrari A C, Flewitt A J, Robertson J, Milne W I, Tagliaferro A and Beyer W 2000 *Diamond Relat. Mater.* **9** 765
[38] Robertson J 1992 *Surf. Coatings Technol.* **50** 185
[39] Pramana D S, Ramachandran K, Venkatramani N, Pandey M and D'Cunha R 2000 *Pramana – J. Phys.* **55** 933
[40] Zhou X T, Lee S T, Bello I, Cheung A C, Chiu D S, Lam Y W, Lee C S, Leung K M and He X M 2000 *Mat. Sci. Eng.* B **77** 229
[41] Martinu L, Raveh A, Boutard D, Houle S and Wertheimer M 1993 *Diamond Relat. Mater.* **2** 673
[42] Zarrabian M, Fourches-Coulon N and Turban G 1997 *Appl. Phys. Lett.* **70** 2535
[43] Kroesen G M W, Timmermans C J and Schram D C 1988 *Pure Appl. Chem.* **60** 795
[44] Benedikt J, Agarwal S, Eijkman D J, Vandamme W, Creatore M and van de Sanden M C M 2005 *J. Vac. Sci. Technol.* A **23** 1400
[45] Gielen J W A M, van de Sanden M C M and Schram D C 1996 *Appl. Phys. Lett.* **69** 152
[46] Benedikt J, Letourneur K G Y, Wisse M, Schram D C and van de Sanden M C M 2002 *Diamond Relat. Mater.* **11** 989
[47] Benedikt J, Woen R V, van Mensfoort S L M, Perina V, Hong J and van de Sanden M C M 2003 *Diamond Relat. Mater.* **12** 90
[48] Benedikt J, Wisse M, Woen R V, Engeln R and van de Sanden M C M 2003 *J. Appl. Phys.* **94** 6932
[49] Benedikt J, Eijkman D J, Vandamme W, Agarwal S and van de Sanden M C M 2005 *Chem.*

Phys. Lett. **402** 37
[50] De Graaf A, van Hest M F A M, van de Sanden M C M, Letourneur K G Y and Schram D C 1999 *Appl. Phys. Lett.* **74** 2927
[51] Philipps V, Vietzke E and Flaskamp K 1986 *Surf. Sci.* **178** 806
[52] Tanaka J, Abrams C and Graves D 2000 *J. Vac. Sci. Technol.* A **18** 938
[53] Brenner D W 1990 *Phys. Rev.* B **42** 9458
[54] Swope W C, Anderson H C, Berens P H and Wilson K R 1982 *J. Chem. Phys.* **76** 637
[55] Berendsen H J C, Postma J P M, van Gunsteren W F, DiNola A and Haak J R 1984 *J. Chem. Phys.* **81** 3684
[56] Neyts E, Bogaerts A and van de Sanden M C M 2006 *Appl. Phys. Lett.* **88** 141922
[57] Neyts E, Bogaerts A and van de Sanden M C M 2006 *J. Appl. Phys.* **99** 014902
[58] Neyts E, Bogaerts A, Gijbels R, Benedikt J and van de Sanden M C M 2004 *Diamond Relat. Mater.* **13** 1873
[59] Neyts E, Tacq M and Bogaerts A 2006 *Diamond Relat. Mater.* **15** 1663
[60] Ferrari A C, Libassi A, Tanner B K, Stolojan V, Yuan J, Brown L M, Rodil S E, Kleinsorge B and Robertson J 2000 *Phys. Rev.* B **62** 11089